waves launched by a small probe in an ion-beam–plasma system. In the system, the direction of the wave propagation vector was found to be not in the radial direction from the launcher. The experimental phase velocity and the spatial growth rate of the slow mode of ion beam were found to be roughly in accord with three-dimensional wave theory. That is, the fastest growing mode was observed in the beam direction for low-velocity ion beams, and for higher velocity, the fastest growing mode was observed in a direction oblique to the ion-beam flow. Moreover, the direction of the fastest growing wave inclines toward the transverse direction with increasing beam velocity.

The authors would like to express their thanks to Professor T. H. Stix for invaluable suggestions in preparing this Letter.

[1]B. D. Fried and A. Y. Wong, Phys. Fluids 9, 1084 (1966).

[2]T. Ohnuma and Y. Hatta, J. Phys. Soc. Jpn. 21, 986 (1966).

[3]D. W. Forslund and C. R. Shonk, Phys. Rev. Lett. 25, 281 (1970).

[4]T. Ohnuma and Y. Hatta, J. Phys. Soc. Jpn. 23, 907 (1967).

[5]A. G. Borishenko, G. M. Kirichenko, and V. G. Fmarque, in Proceedings of the Fourth International Conference on Plasma Physics and Controlled Nuclear Fusion Research, Madison, Wisconsin, 1971 (International Atomic Energy Agency, Vienna, Austria, 1972).

[6]T. Ohnuma, T. Fujita, and Y. Hatta, Phys. Lett. 36A, 265 (1971).

[7]R. W. Means, F. V. Coroniti, A. Y. Wong, and R. B. White, Phys. Fluids 16, 2304 (1973).

[8]Y. Kiwamoto, J. Phys. Soc. Jpn. 37, 466 (1974).

[9]D. R. Baker, Phys. Fluids 16, 1730 (1973).

[10]T. Fujita, T. Ohnuma, and S. Adachi, Phys. Fluids 18, 1216 (1975).

[11]R. J. Taylor and F. V. Coroniti, Phys. Rev. Lett. 29, 37 (1972).

[12]T. Ohnuma, T. Fujita, and S. Adachi, Phys. Rev. Lett. 31, 1177 (1973).

[13]For example, T. H. Stix, Theory of Plasma Waves (McGraw-Hill, New York, 1962), Chap. 3.

[14]For example, H. H. Kuehl, Phys. Fluids 16, 1311 (1973).

[15]B. D. Fried and S. D. Conte, The Plasma Dispersion Function (Academic, New York, 1961).

[16]M. J. Lighthill, Philos. Trans. Roy. Soc. London, Ser. A 252, 397 (1960).

[17]Recently, D. Grésillon, F. Doveil, and J. M. Buzzi reported theoretical results similar to Fig. 3(b) in Phys. Rev. Lett. 34, 197 (1975).

Simulation of Dissipative Trapped-Electron Instability in Linear Geometry*

Y. Matsuda and H. Okuda

Plasma Physics Laboratory, Princeton University, Princeton, New Jersey 08540

(Received 22 December 1975)

A simulation model has been developed to study the low-frequency trapped-particle instability in a linear geometry. Low-frequency drift instabilities identified as the dissipative trapped-electron modes grow, accompanied by the turbulent transport of plasma. Measured electron heat conductivity is a few times larger than the particle diffusion constant.

Low-frequency microinstabilities such as drift-wave and trapped-particle instabilities have been of wide interest in relation to research on controlled thermonuclear fusion in low-density magnetic-confinement systems. While there is certain experimental evidence that these low-frequency instabilities may be responsible for the anomalous plasma transport in both linear geometry[1] and toroidal systems,[2] positive identification of the instability and the scaling of the associated plasma transport are difficult in many cases where the experimental situation is far more complex than the theoretical treatments.

As for the trapped-electron instability, several experiments have been performed in linear devices for the identification of the instability.[1] It is, however, very difficult to measure cross-field transport in linear devices since the motion along the field lines is much faster than the cross-field diffusion. In a toroidal system it is possible to measure the cross-field transport; extensive investigations on plasma transport have been carried out for the FM-1 spherator.[2]

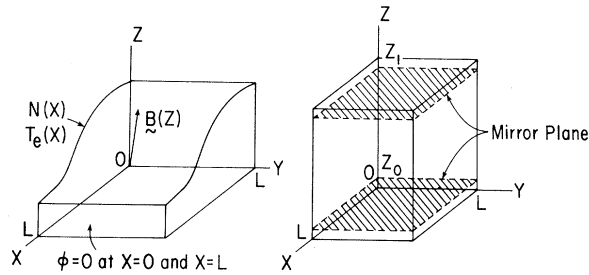We have developed a simulation model shown

FIG. 1. A sketch of the simulation model.

in Fig. 1 to study the trapped-electron instability in a linear geometry. The density and the temperature are nonuniform in the x direction where the plasma is confined between two conducting plates located at $x = 0$ and $x = L$.[3] In the y direction, the plasma is assumed uniform and period-

ic. In the z direction, the plasma is also assumed periodic. The mirroring field is mocked up by the reflection of particles along the field lines depending on the magnitude of $v_\parallel$ and $v_\perp$ for each particle at the planes $z = z_0$ and $z = z_1$, which are assumed to be the same plane because of the periodicity of the model. Monte Carlo collisions are used to model the electron pitch-angle scattering with the ions.[4] Although some simulations were carried out using a full three-dimensional code, most of the runs are with a $2\frac{1}{2}$-dimensional code. For the $2\frac{1}{2}$-dimensional simulations which we report here, a small but finite angle is required between the magnetic field and the z axis in order to couple the particle bounce motion with the wave electric field in the y direction. This will introduce a finite, but small, $k_\parallel$ in the model.

The dissipative trapped-electron instability in the original treatment of Kadomtsev and Pogutse[5] is described by the dispersion equation

$$1 - \frac{\omega^*}{\omega} - \frac{k_\parallel^2 T_e}{m_i \omega^2} - \epsilon^{1/2} \int \frac{\omega - \omega_*[\,1 + \eta_e(v^2/v_e^2 - \frac{3}{2})\,]}{\omega + i\nu_e v_e^3/\epsilon v^3} f_M \, d^3v = 0, \tag{1}$$

where f_M is the Maxwellian electron distribution function, ϵ is the inverse aspect ratio, ν_e is the electron collision frequency, v_e is the electron thermal speed, $\omega_* = - ck_y T_e (dn/dx)/eBn$ is the electron drift frequency, and $\eta_e = d\ln T_e/d\ln n$ is the ratio of the temperature gradient to the density gradient. It is assumed in the derivation of Eq. (1) that $\omega_{bi} < \omega < \omega_{be}$, where ω_{bi} and ω_{be} are the ion and electron bounce frequencies, respectively. Equation (1) predicts an instability for $\omega \sim \omega_* \lesssim \nu_e/\epsilon$ with growth rate $\gamma \simeq \epsilon^{3/2} \eta_e \omega_*^2/\nu_e$.

Typical simulation parameters are the following: 64×64 mesh, 2^{15} particles for each species, mass ratio $m_i/m_e = 100$, temperature ratio $T_e/T_i = 16$, electron gyrofrequency $\Omega_e/\omega_{pe} = 2$, and Debye length $\lambda_D/\Delta = 0.5$. These parameters give the system size $L/\rho_i = 25$ and $L/\lambda_D = 128$. Here ω_{pe}, Δ, and ρ_i are the electron plasma frequency, the mesh size, and the ion gyroradius. The initial density profile is taken as $N(x) = n\{1 - \alpha_N \times \tan[(x - L/2)/L_N]\}$ with $\alpha_N \simeq 0.82$ and $L_N/\rho_i \simeq 4.5$. The initial electron temperature profile is chosen similarly with α_T and L_T replacing α_N and L_N to provide the appropriate value of η_e near $x = L/2$. The ion temperature is taken to be uniform initially. Typically we used $\omega_{be}/\omega_{pe} \simeq 0.2$, $\nu_e/\omega_{pe} \simeq 0.04$, and $\omega/\omega_{pe} \simeq 0.02$–$0.04$. The ions are not reflected so that $\omega_{bi} = 0$. The depth of the mirror-

ing field is chosen so that the inverse aspect ratio ϵ is approximately 0.25.

Let us now look at the results of simulations. Included are the cases $\eta_e > 0$, $\eta_e = 0$, and $\eta_e < 0$ with various collision frequencies. Figure 2(a) shows the density modulation $\delta n/n_0$ averaged over x. For a short time, small-scale perturbations are excited which saturate rather quickly followed by the large-scale perturbations ($k_y \rho_i = 0.25$ and 0.5). These large-wavelength modes grow to very large amplitudes ($\delta n/n_0 \approx 15\%$) at approximately the expected growth rate: The measured growth rate is $\gamma/\omega_{pe} \approx 0.003$ for $k_y \rho_i = 0.25$ which is in reasonable agreement with a solution of the dispersion equation including the correction for finite ion gyroradius. Associated with the density perturbations are electric field fluctuations which cause large diffusion of particles and heat. The growth of the electric field is plotted in Fig. 2(b) for three different temperature gradients. For $\eta_e = 1.5$, which corresponds to the conventional trapped-electron instability, the electric field fluctuations grow above the high-frequency noise level at $\omega_{pe} t \approx 2000$ saturating at about $\omega_{pe} t \approx 3000$. The other two runs, $\eta_e = 0$ and $\eta_e = -1.0$, were carried out to confirm the trapped-electron instability. For $\eta_e = 0$, we observe an instability
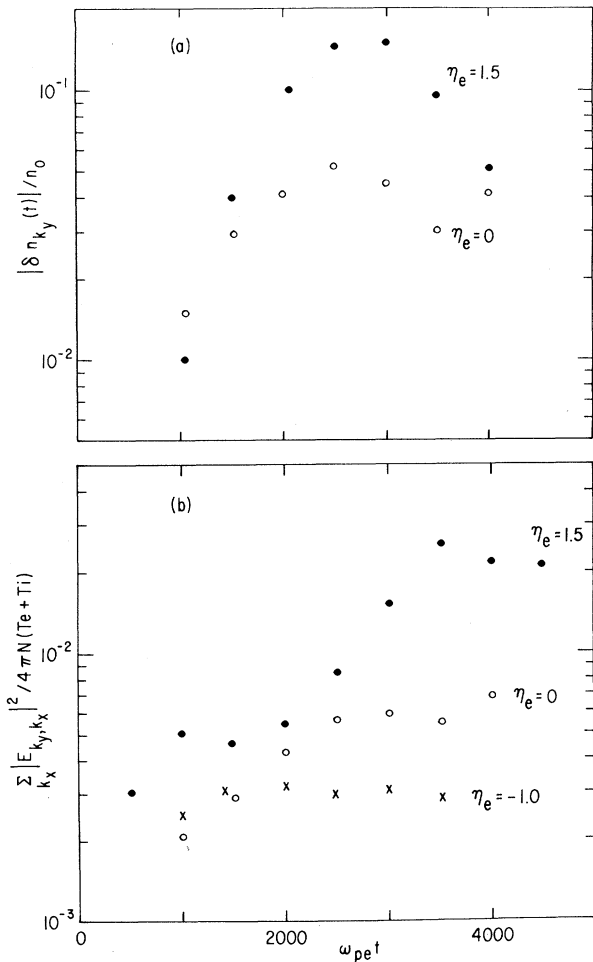
FIG. 2. Growth of (a) the density perturbation, and (b) the electric field fluctuation of mode $k_y \rho_i = 0.25$ for the cases $\eta_e = 1.5$, 0, and -1.0.

FIG. 3. Time evolution of the profile of (a) the particle density $N(x)$ and (b) the fluctuation potential $\varphi(x)$ for the case $\eta_e = 1.5$.

growth which corresponds to the density modulation shown in Fig. 2(a), but which saturates at a lower level than for $\eta_e = 1.5$. This probably corresponds to the trapped-electron instability driven by the finite ion gyroradius.[6] For $\eta_e = -1.0$, there are essentially no instabilities observed. Although these results positively identify the trapped-electron instability, one more confirmation was tried for the case $\eta_e = 1.5$ by deleting the collision operator from the simulations. It was observed that the fluctuations as well as the anomalous diffusion immediately disappered.

In Fig. 3, the density profile and the mode structure of the wave potential in the x direction are shown at different times for the case $\eta_e = 1.5$. The density profile begins changing significantly at $\omega_{pe} t \approx 2200$ where the electric field fluctuations
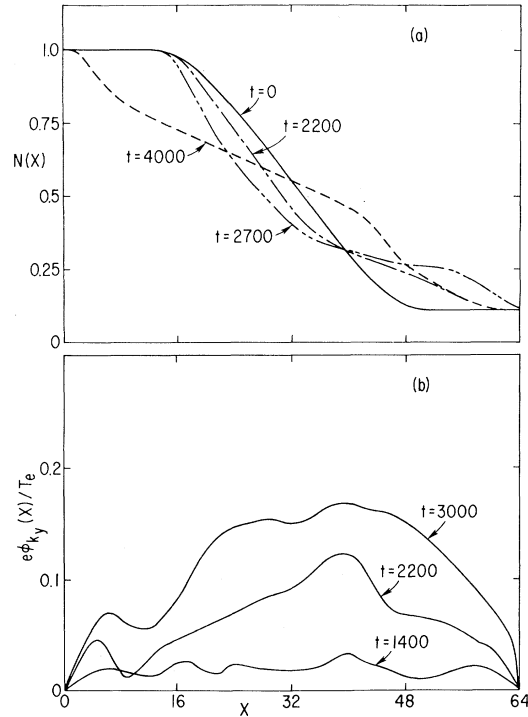
grow beyond the noise level as shown in Fig. 2. Indeed, the mode structure also indicates a coherent profile at this time. We see that the initial random fluctuations are dominated by the more coherent wave profile peaked at the center of the plasma column, growing to a large amplitude and at the same time spreading radially.

The mode structure is similar to what was observed for the collisionless drift-wave turbulence.[7] The particle diffusion, on the other hand, indicates a significant difference at the nonlinear stage of the instability. The quasilinear plateau in the local density profile, which was identified as the stabilization mechanism for the collisionless drift-wave turbulence, is not clearly observed for the present simulations.

Figure 4 shows the particle and heat diffusion in the x direction for three different temperature gradients obtained by using the Fourier-expansion method.[8] For $\eta_e = 1.5$, we observe that the temperature decays a few times faster than does the density. The temperature gradient is reduced over 50% by the time of saturation. Assuming a diffusion equation for the density and the temperature, i.e., $\partial N/\partial t = D_\perp \partial^2 N/\partial x^2$ and $\partial T_e/\partial t = \kappa^e \partial^2 T_e/$

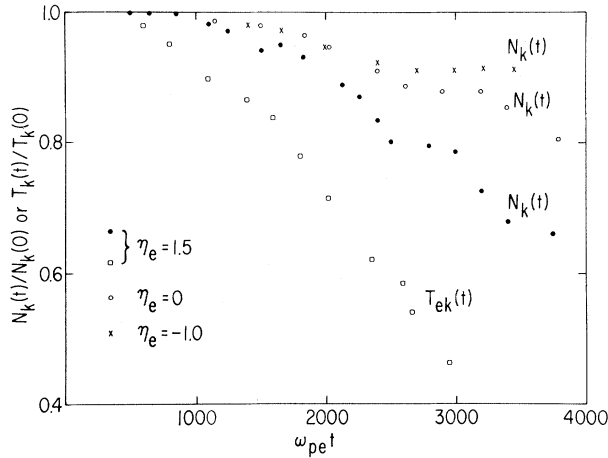FIG. 4. Decay of the density and temperature profiles with time.

∂x^2, it is straightforward to evaluate $D_\perp$ and κ^e from Fig. 4. One finds $D_\perp \simeq 0.013\Delta^2\omega_{pe}$ and $\kappa^e \simeq 0.027\Delta^2\omega_{pe} \simeq 2D_\perp$ for the case $\eta_e = 1.5$. One interesting observation regarding the heat transfer is that the parallel temperature $T_{e\parallel}(x)$ decays more slowly than the perpendicular temperature $T_{e\perp}(x)$. This is similar to what was observed for the simulation of collisionless drift waves.[7] The mechanism for the different heat-transfer rates is that while $T_{e\perp}(x)$ decays as the result of particle diffusion across the magnetic field, the diffusion of $T_{e\parallel}(x)$ is compensated somewhat because of the wave energy transfer associated with the radial propagation of waves from the unstable region to the region of higher plasma temperature.[7,8] The measured ratio, $\kappa^e/D_\perp \simeq 2$, which is somewhat smaller than expected,[5] is probably due to this wave energy transfer. In fact, if we calculate the heat conductivity from $T_{e\perp}(x)$, we obtain $\kappa_\perp^e/D_\perp \simeq 3 - 4$.

Let us now discuss the saturation of the instability for the case $\eta_e = 1.5$. As seen in Fig. 4, the temperature diffusion is a few times as fast as that of the density. Indeed, the temperature gradient becomes quite small at the time of saturation at around $\omega_{pe}t = 3000$, which appears to have led to the saturation of the instability. No quasilinear effect was observed in the electron velocity space in contrast to the collisionless drift-wave instability.[7] This is because the rapid electron collisions tend to maintain the Maxwellian distribution. In fact, it appears possible to explain the nonlinear evolution of the instability observed in the present simulation in terms of the quasilinear theory for the macroscopic den-

sity and the temperature including Coulomb collisions and turbulence.[9] While the plasma could still be unstable against the finite-gyroradius instability after the flattening of the temperature, the instability appeared to have saturated. The turbulence could have quenched the weaker instability.

There are other possible mechanisms for the nonlinear saturation of this instability.[10] One of them is the detrapping of the trapped electrons from the magnetic mirror by the turbulent electric field. This requires an electric field potential φ such that $e\varphi/T_e \gtrsim \delta B/B \simeq 0.25$ which is to be compared with the observed saturation level $e\varphi/T_e \approx 0.15$ as shown in Fig. 3. As shown earlier, quasilinear diffusion stabilizes the instability before the fluctuations become so large that detrapping takes place. Another is nonlinear mode coupling. However, no evidence has been observed in the present simulations to indicate this as the saturation mechanism. We believe that this is because the strongly unstable modes are such that $k_y\rho_i \approx 0.5$ for which the propagation is highly dispersive.

Finally, we note that the usual estimate of diffusion $D_\perp \simeq \gamma/k_\perp^2 \simeq \gamma/k_y^2 \simeq 0.3\Delta^2\omega_{pe}$ is much larger than the observed diffusion $D_\perp \simeq 0.013\Delta^2\omega_{pe}$. This is partly because the saturation was provided by flattening of the temperature profile before the density profile changed significantly. $\gamma/k_\perp^2$ should, therefore, be compared with $\kappa_\perp^e \simeq 0.05\Delta^2\omega_{pe}$. The details of the quasilinear theory will be reported elsewhere.

It is a pleasure to acknowledge discussions with Dr. J. C. Adam, Dr. M. Okabayashi, and Dr. W. M. Tang.

[1]P. Deschamps, R. Gravier, C. Renaud, and A. Samain, Phys. Rev. Lett. 31, 1457 (1973); S. C. Prager, A. K. Sen, and T. C. Marshall, Phys. Rev. Lett. 33, 692 (1974).
[2]S. Ejima and M. Okabayashi, Phys. Fluids 18, 904 (1975).
[3]W. W. Lee and H. Okuda, to be published.
[4]R. Shanny, J. M. Dawson, and J. M. Greene, Phys. Fluids 10, 1281 (1967).
[5]B. B. Kadomtsev and O. P. Pogutse, Dokl. Akad. Nauk SSSR 186, 553 (1969) [Sov. Phys. Dokl. 14, 470 (1969)].

[6]C. S. Liu, M. N. Rosenbluth, and W. M. Tang, Princeton Plasma Physics Laboratory Report No. MATT-1125, 1975 (unpublished).

[7]W. W. Lee and H. Okuda, Princeton Plasma Physics Laboratory Report No. MATT-1188 (to be published);

also private communication with M. True.

[8]J. Canosa and H. Okuda, Phys. Fluids 18, 335 (1975).

[9]Y. Y. Kuo, to be published.

[10]B. B. Kadomtsev and O. P. Pogutse, Nucl. Fusion 11, 67 (1971).

$T^{3/2}$ Contribution to the Specific Heat of Ferroelectrics at Low Temperatures

W. N. Lawless

Corning Glass Works, Research Laboratory, Corning, New York 14830

(Received 1 December 1975)

A $T^{3/2}$ contribution to the low-temperature specific heat of the ferroelectrics triglycine sulfate, potassium dihydrogen phosphate, $BaTiO_3$, and $LiNbO_3$ is reported. This may be a domain-wall contribution because it is not present in paraelectrics or antiferroelectrics.

The specific heats of a number of well-known paraelectrics, ferroelectrics, and antiferroelectrics have been measured in an adiabatic vacuum calorimeter in the range 2–35 K.[1] This Letter reports an unusual contribution to the specific heat found only in the ferroelectrics at the lowest temperatures.

All of the materials measured show maxima in CT^{-3} ($5.3 \leqslant T_{max} \leqslant 26.3$ K), and these maxima can be fitted very well with single Einstein frequencies.[1] At temperatures below T_{max}, the CT^{-3} curves for the paraelectrics and antiferroelectrics decrease with decreasing temperature and approach the flat T^3 Debye behavior. For the *ferroelectrics*, however, the CT^{-3} curves go through minima and *increase* with decreasing temperature down to 2 K. The measuring conditions ($< 5\%$ uncertainty) and addenda were essentially the same for the paraelectrics, ferroelectrics, and antiferroelectrics.[1]

The specific-heat data below the CT^{-3} minima for the ferroelectrics follow very accurately a $T^{3/2}$ law,

$$C = AT^3 + BT^{3/2}, \qquad (1)$$

as shown in Fig. 1 for the displacive ferroelectrics $BaTiO_3$ and $LiNbO_3$ and in Fig. 2 for the hydrogen-bonded ferroelectrics potassium dihydrogen phosphate (KDP) and triglycine sulfate (TGS). The samples were multidomain single crystals (no attempt was made to pole the crystals).

The data in Figs. 1 and 2 were fitted by Eq. (1) and the results are summarized in Table I. The Debye temperatures in Table I were calculated from the coefficient A, and confidence limits are given on the B coefficient.

The excellent data fits leave no doubt as to the presence of the $T^{3/2}$ term and the presence of this term depends on whether the crystal is ferroelectric or not rather than whether the ferroelectric is displacive or hydrogen bonded. It is natural to ascribe this $T^{3/2}$ contribution to the presence of domain walls.

One would expect the B coefficient in Eq. (1) to be proportional to the number of domain walls present in the crystal; this can be controlled by
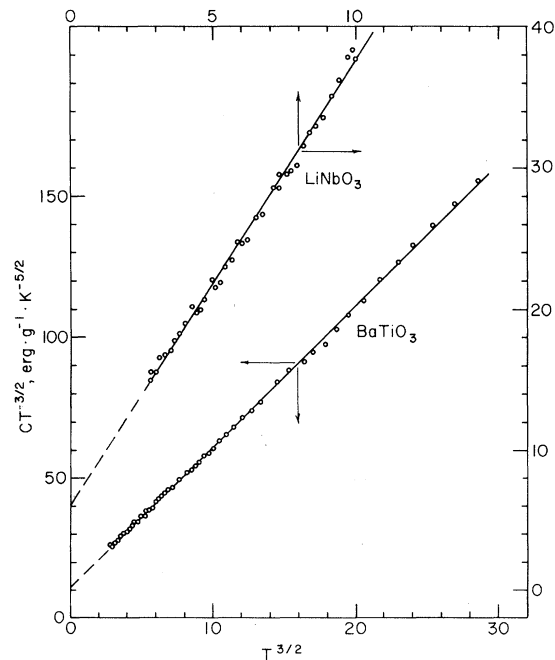

FIG. 1. Specific-heat plot according to Eq. (1) for the displacive-type ferroelectrics $BaTiO_3$ and $LiNbO_3$.